ISSN: 2621-4709 E-ISSN: 2621-2528
Journal of Applied Agricultural Science and Technology
Vol. 10 No. 3 (2026): 543-563

Drying Performance and Computational Fluid Dynamics Analysis of a Circular-Pipe Conical-Floor Paddy In-Store Dryer

Diswandi Nurba [a,*], Muhammad Yasar [a], Dyah Wulandani [b]

[a] Department of Agricultural Engineering, Universitas Syiah Kuala, Banda Aceh, Indonesia
[b] Department of Mechanical and Biosystem Engineering, IPB University, Bogor, Indonesia

Abstract. *The in-store dryer (ISD) is a well-established convective drying-storage system; however, conventional designs often suffer from uneven airflow distribution and inefficient heat transfer. To address this gap, this study introduces a novel configuration featuring a circular-pipe conical floor and an improved hot-air supply arrangement through axial-blower repositioning and inlet-air regulation to enhance airflow uniformity. Drying experiments were conducted using 300 kg of paddy over an 8-h drying period. The measured operating condition was then applied as the boundary condition for Computational Fluid Dynamics (CFD) simulation. The improved ISD maintained relatively stable drying conditions, with a mean chamber temperature of 37.13 °C, internal RH of 57.32%, and an inlet airflow rate of 0.66 $m^3 s^{-1}$ (corresponding to a velocity of 5.35 $m s^{-1}$ during blower operation). Paddy moisture content decreased from 17.78% to 10.44% (w.b.), corresponding to an apparent moisture reduction rate of 0.92 percentage points h^{-1}. The estimated total specific energy consumption was 20.98 MJ kg^{-1} water evaporated. CFD validation, performed by comparing simulated data with measured values at specific sensor points inside the drying chamber, showed acceptable to good agreement, with RMSE values of 0.54 °C for temperature, 1.73% for RH, and 0.38 $m s^{-1}$ for airflow velocity, and correlation coefficients of 0.81, 0.76, and 0.84, respectively. These results indicate that the improved ISD achieved effective bulk paddy drying and that the validated CFD model adequately represented the internal airflow and thermal-humidity behavior of the system.*

Keywords: *airflow distribution; bulk grain storage; CFD validation; heat exchanger; post-harvest technology.*

Type of the Paper: Regular Article.

1. Introduction

Paddy drying is a key postharvest operation because grain moisture content affects storability, milling quality, and resistance to deterioration during storage and processing [1,2]. In many rice-producing regions, drying process still faces challenges from fluctuating ambient conditions, uneven airflow distribution, and limited access to efficient mechanical dryers [2–4]. These constraints often cause non-uniform moisture reduction, extended drying times, and unstable product quality [3,4]. Therefore, drying systems that combine effective moisture removal, practical energy use, and operational simplicity remain relevant in agricultural engineering [2,3,5].

An in-store dryer (ISD) integrates drying and storage into a single convective system [6–8]. This arrangement allows gradual drying to a safer moisture level and facilitates storage within the

https://doi.org/10.55043/jaast.v10i3.589
Received April 21, 2026; Received in revised form July 11, 2026; Accepted July 21, 2026; Published August 21, 2026
* Corresponding author
Email: diswandinurba@usk.ac.id

same chamber [7,8]. It is suited for second-stage drying, in which grain with moderately high moisture content is further dried toward equilibrium moisture content before longer-term storage [2,7]. However, ISD performance depends on the quality and distribution of drying air inside the grain mass [6,7,9]. In deep-bed systems, poor airflow distribution can create non-uniform temperature and humidity fields, causing grain near the air inlet to dry faster than that in upper or remote zones [4,9–11]. Consequently, moisture gradients may persist, reducing drying effectiveness and affecting grain quality [4,9,12]. To mitigate these issues, structural modifications such as a circular-pipe conical-floor arrangement can be employed. This specific geometry offers significant engineering relevance as it is theoretically designed to minimize pressure loss, optimize upward air distribution, and ultimately enhance drying uniformity across the grain bed.

Beyond structural geometry, drying performance is driven by inlet-air conditions, specifically temperature, relative humidity (RH), and airflow velocity [13–16]. While ambient air is often utilized for aeration in tropical regions, its typically high and fluctuating relative humidity severely limits its drying potential [16,17]. Relying solely on ambient air without proper control can lead to unstable drying and grain deterioration [13,14,16]. Thus, inlet air must be managed in terms of thermal condition and flow rate through supplemental heating [13,15,18]. In biomass-assisted systems, this is even more critical because useful heat delivered to the chamber depends not only on the heat source, but also on heat-exchanger configuration and airflow delivery [14,15,19]. Recent studies show that energy performance, thermal effectiveness, and drying behavior are closely linked to how heated air is generated and distributed [5,14,15,19].

To improve inlet-air delivery, ISD systems commonly use a heat exchanger and a blower [5,6,20]. The heat exchanger raises air temperature above ambient level, while the blower conveys heated air into the plenum and drying chamber [5,6,20]. However, if blower arrangement is not optimal, generated heat may be lost before reaching the grain bed [5,9,20–22]. This study addressed that issue by modifying axial-blower position to improve heated-air delivery and reduce heat loss. The control system was also refined using multiple temperature and RH sensors inside and outside the ISD, so airflow decisions were based on averaged rather than single-point measurements. This approach was intended to provide a more representative assessment of drying conditions and a more suitable airflow supply for paddy drying [9,23].

Sensor- and model-based control of drying air is well established in grain drying systems [23,24]. Earlier work showed that online detection and model-based control can improve drying management and reduce unnecessary energy use [23]. More recent studies have extended this direction toward intelligent or predictive control for grain and paddy dryers, including support-vector-regression-based inverse-model PID control and deep-learning-based model predictive control [24,25]. Even so, practical agricultural dryers still require robust systems that can operate under field conditions with relatively simple hardware and control logic [18,20]. Therefore, combining heat-exchanger-assisted air heating with sensor-based airflow control remains a practical engineering solution for paddy drying [14,20,23,24].

Computational fluid dynamics (CFD) has become a key tool for analyzing airflow distribution, temperature fields, and internal transport behavior in agricultural dryers [4,9–11,26]. Recent studies on paddy drying have applied CFD and related numerical approaches to evaluate airflow uniformity, chamber design, and heat-mass transfer behavior [4,9–11,26,27]. These methods are especially useful in deep-bed and chamber-type dryers, where internal flow pathways are strongly affected by geometry and air-distribution structures [4,9–11]. However, CFD-oriented studies mainly analyze internal flow fields or design alternatives, whereas many experimental studies focus primarily on moisture reduction, energy use, and product quality [3,5,14,20,28]. Consequently, the explicit linkage between measured operating conditions and chamber-scale airflow behavior remains limited [4,5,9–11,14,20]. Specifically, previous studies have insufficiently integrated experimental drying data with CFD boundary conditions. Furthermore, validation using measured chamber data, particularly for a circular-pipe conical-floor ISD configuration, remains largely unexplored.

This study addresses this gap by integrating experimental drying performance with CFD-based airflow analysis for the aforementioned circular-pipe conical-floor ISD for paddy. This configuration is relevant because air-distribution geometry strongly affects how inlet air propagates through the drying chamber and interacts with the grain bed [9–11]. Rather than using CFD as a stand-alone design tool, this study uses experimentally measured operating conditions as boundary conditions for numerical analysis. CFD is therefore employed to interpret how the controlled inlet-air condition is distributed inside the chamber and how that distribution supports bulk drying performance.

The novelty of this study lies in the linkage between experimentally measured controlled operating conditions of an improved paddy in-store dryer and CFD-based internal airflow analysis, connecting heat-exchanger-assisted inlet-air management to chamber-scale drying behavior in a circular-pipe conical-floor configuration. Accordingly, this study aimed to evaluate the controlled drying performance of this ISD and interpret airflow behavior using CFD, focusing on thermal-airflow characteristics, bulk moisture reduction, energy requirement, and airflow distribution.

2. Materials and Methods

2.1 In-store dryer configuration

The dryer used in this study was a cylindrical in-store dryer (ISD) designed for paddy drying. The structural configuration of the improved ISD is shown in Fig. 1. The unit had a total height of

1.65 m, a diameter of 0.80 m, and an insulated wall thickness of 0.04 m (consisting of inner and outer layers with glass wool insulation in between them). The system was equipped with a top loading opening with a diameter of 0.30 m, which also functioned as the upper air outlet, a lower paddy discharge outlet, a plenum chamber, a heat exchanger, an axial blower, and a biomass furnace. The heating unit comprised a biomass furnace positioned directly below a cross-flow multi-tube heat exchanger (0.4 × 0.35 × 0.35 m). This heat exchanger was equipped with a matrix of 36 horizontal heating tubes (34 mm) designed to completely isolate the clean drying air from the combustion flue gases rising from the furnace.

Internally, the air-distribution system consisted of a conical floor, nine inlet air pipes, and four outlet air pipes. Detailed engineering specifications of these internal components included a conical-floor angle of 38°, a plenum volume of 0.10 m^3, inlet pipes with a diameter of 0.08 m and a length of 0.80 m, and outlet pipes with a diameter of 0.12 m and a length of 0.80 m. The entire air-distribution pipe system and the conical floor were constructed from perforated metal plates featuring a perforation diameter of 2 mm and an open-area ratio of 32.65%. With these structural dimensions, the effective chamber volume was 0.63 m^3 (which specifically refers to the usable grain-holding volume rather than the total geometric cylinder volume). During the experiments, the dryer was loaded with 300 kg of paddy, resulting in a grain-bed depth of 0.92 m and a bulk density of 522 kg m^{-3}. Operationally, the inlet air pipes passed directly through the perforated conical floor to receive drying air from the plenum chamber, distributing it radially throughout the grain bulk. The outlet air pipes, suspended within the paddy bulk, captured the moist air released from the grain bed and conveyed it toward the upper air outlet.

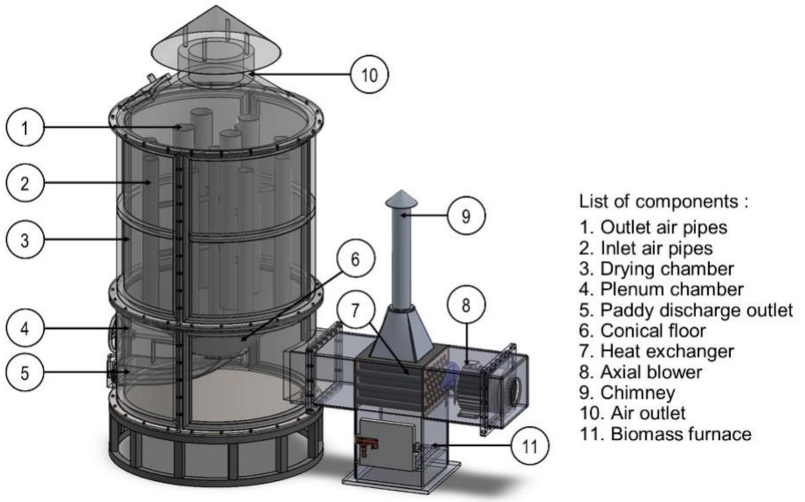

Fig. 1. Structural configuration of the improved cylindrical in-store dryer (ISD) for paddy drying.

The ISD evaluated in this study represents an improved configuration derived from a previously developed system. In the earlier configuration, the axial blower was positioned between the ISD chamber and the heat exchanger and functioned to draw and deliver heated air into the dryer. However, this arrangement had not yet been equipped with an active regulation system and was associated with heat loss and fluctuations in the supplied-air temperature [6]. In the improved configuration, the axial blower was relocated to the rear side of the heat exchanger to reduce heat loss and improve hot-air delivery into the plenum chamber and drying chamber. The system was also equipped with an Arduino-based inlet-air regulation system. The blower was activated when the estimated equilibrium moisture content (EMC) of the drying air was lower than the measured paddy moisture content and deactivated when the drying potential was insufficient. Airflow speed was adjusted using an electronic dimmer according to predefined temperature–RH thresholds. Specifically, the regulation system dynamically modulated the blower to operate at three nominal inlet-air velocities: 5.0 m s^{-1} (low mode), 5.5 m s^{-1} (medium mode), and 6.0 m s^{-1} (high mode). Thus, the improved ISD integrated both axial-blower rearrangement and inlet-air regulation to provide a more stable hot-air supply.

2.2 Instrumentation and measurement uncertainty

Temperature and relative humidity (RH) profiles were continuously monitored to capture both the internal drying conditions (within the plenum chamber and grain bulk) and the external ambient environment. The measured variables included ambient temperature, ambient RH, internal ISD temperature, internal ISD RH, inlet airflow velocity, and chimney airflow velocity. Inlet-air velocity was measured using a Climomaster anemometer (Model 6501, Kanomax) positioned at the center of the air inlet duct. The volumetric airflow rate was calculated by multiplying the mean velocity by the inlet cross-sectional area and was expressed as m^3 min^{-1} and m^3 min^{-1} kg^{-1} paddy.

To ensure data reliability, measurement uncertainty and instrument accuracy were strictly documented based on the manufacturer's specifications. Thermal profiling across the dryer was recorded using K-type thermocouples connected to a Graphtec Midi Logger GL240, with a temperature accuracy of ±(0.05% of reading + 1.0 °C). For the Arduino-based control system, environmental monitoring was performed using DHT22 sensors, providing a temperature accuracy of ±0.5 °C and an RH accuracy of ±2%. The Kanomax 6501 anemometer used for airflow measurement had an accuracy of ±2% of the reading or 0.015 m s^{-1}. Sample mass determination during the drying trials was conducted using an A&D analytical balance (Model FX-3000i) with a precision of ±0.01 g. Grain moisture content was evaluated using a Crown Digital Grain Moisture Meter (Model TA-5) with an accuracy of ±0.5%. Furthermore, electrical energy parameters were measured using a digital clamp meter (Model UT201, UNI-T) operating with an accuracy of ±(1.2% + 5 digits). Operational data from the drying trials were recorded and later summarized to characterize the operating condition of the improved system. The airflow pathway of the improved ISD and the spatial arrangement of the observation points used for these measurements are illustrated in Fig. 2.

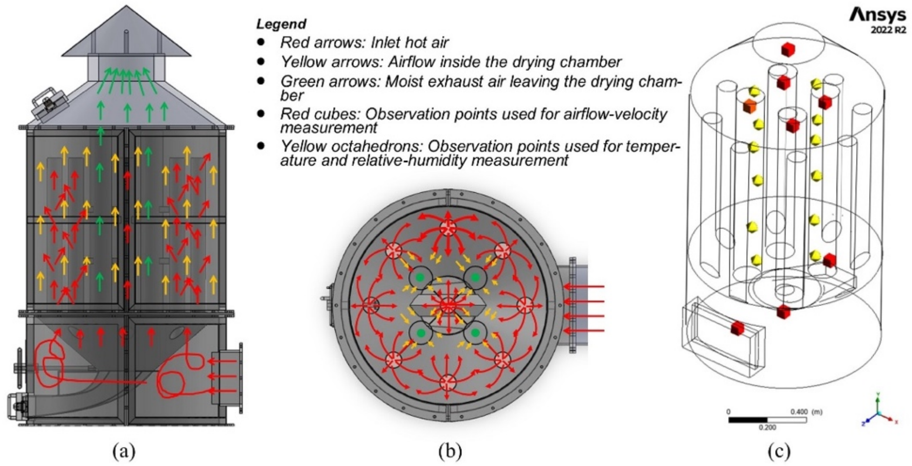

Fig. 2. Airflow pathway of the improved ISD and CFD validation domain: (a) side view of the airflow pathway, (b) top view of the airflow pathway, and (c) CFD computational domain showing the representative observation points used for simulation and validation.

2.3 Drying material and experimental procedure

Paddy was used as the drying material. Each drying test used 300 kg of paddy with an initial moisture content of approximately 18% (w.b.), while wood charcoal biomass served as the heat source for the heat exchanger. Throughout the drying process, the wood charcoal fuel, having an estimated lower heating value (LHV) of 23.61 MJ kg^{-1} and a moisture content of approximately 8.5%, was manually fed in batches by an operator to maintain the target drying air temperature. Fuel consumption during the drying process was measured quantitatively using a mechanical platform scale.

Three independent drying trials were conducted using separate 300 kg paddy batches. The paddy was loaded into the chamber as a bulk bed and dried for 8 h (09:00–17:00). During the drying process, rapid preliminary checks of grain moisture, such as determining the initial condition and identifying the final operational shutdown point, were conducted in situ using the Crown Digital Grain Moisture Meter. However, for accurate data reporting and drying-rate calculations, the definitive moisture content was determined using the standard oven-drying method at 105 °C for 24 h, following the ASABE S352.2 standard. Samples of approximately 15 g were collected from the lower, middle, and upper layers of the grain bed at 2-h intervals. All moisture content values are expressed on a wet basis (w.b.). Results are presented as mean ± standard deviation unless otherwise stated.

Temperature and relative humidity were monitored continuously by the control system using sensors installed within the grain bulk and in the ambient air of the ISD, with data recorded at 1-min intervals. Inlet airflow velocity, chimney airflow velocity, electrical energy consumption, and biomass use were also recorded during drying. Because the study focused on the overall drying behavior of the improved system, drying performance is presented mainly in terms of bulk moisture reduction, drying rate, and energy-performance indicators.

2.4 Performance calculations

The drying performance of the ISD was evaluated based on the reduction in paddy moisture content during the drying period. Moisture content was recorded at several observation times during each drying trial. Initial moisture content, final moisture content, and the temporal reduction in bulk moisture content were used to describe the drying process. The apparent drying rate was calculated using Eq. (1) [7,8].

$$DR_a = \frac{MC_i - MC_f}{t} \tag{1}$$

where DR_a is the apparent drying rate (% h^{-1}), MC_i is the initial moisture content (%), MC_f is the final moisture content (%), and t is the drying time (h).

In addition to the apparent drying rate, a mass-based drying rate was also calculated from the amount of water removed during drying using Eq. (2) [8].

$$DR_m = \frac{m_{ev}}{t} \tag{2}$$

where DR_m is the mass-based drying rate (kg H_2O h^{-1}), m_{ev} is the mass of water evaporated during drying (kg), and t is the drying time (h).

The mass of evaporated water was determined from the difference between the initial and final water content of the paddy load. In addition to the overall average drying rate, interval drying rates were also determined from the reduction in moisture content over each observation interval to evaluate the variation in drying intensity during the 8-h drying process.

The energy requirement of the controlled ISD was evaluated using two components: electrical energy consumption and biomass consumption. Electrical energy was recorded as the electricity used during the drying process, while biomass consumption represented the fuel required to operate the heat exchanger. The electrical requirement was reported in kWh per process, whereas biomass use was reported in kg per process. Where applicable, biomass energy input was expressed using the energy value associated with the recorded fuel consumption.

In addition to direct energy use, specific energy consumption (SEC) and specific moisture extraction rate (SMER) were used as indicators of drying energy performance [2,29]. The total specific energy consumption was calculated using Eq. (3).

$$SEC = \frac{E_{tot}}{m_{ev}} \tag{3}$$

where SEC is the specific energy consumption (MJ kg^{-1} water evaporated), E_{tot} is the total energy input (MJ), and m_{ev} is the mass of water evaporated during drying (kg).

The total energy input was obtained from the sum of electrical energy input and biomass energy input. The electrical energy input was calculated by converting electrical consumption from kWh to MJ.

The specific moisture extraction rate based on electrical energy was calculated using Eq. (4) [29].

$$SMER = \frac{m_{ev}}{E_{elec}} \quad (4)$$

where *SMER* is the specific moisture extraction rate (kg H_2O kWh^{-1}), m_{ev} is the mass of water evaporated during drying (kg), and E_{elec} is the electrical energy consumption during the drying process (kWh). These indicators were used to evaluate the energy performance of the improved ISD under controlled drying conditions.

2.5 CFD simulation setup

Computational fluid dynamics (CFD) was employed to simulate the internal airflow behavior of the circular-pipe conical-floor in-store dryer (ISD) under the tested operating condition. The CFD model was used to predict the distribution of air velocity, temperature, and relative humidity within the drying chamber and grain bed. The computational domain and representative observation points used for simulation and validation are shown in Fig. 2(c). The domain included the main internal components of the improved ISD, namely the plenum chamber, perforated inlet air pipes, perforated conical floor, drying chamber, suspended outlet air pipes, and the upper air outlet.

The numerical simulation was conducted using Ansys Fluent 2022 R2 software. A pressure-based solver was utilized to solve the governing equations of mass (continuity), momentum, and energy under steady-state conditions. Turbulence within the airflow was resolved using the standard k-ϵ turbulence model. The paddy bulk was explicitly treated as a homogeneous porous medium governed by the Darcy-Forchheimer law. Porosity, permeability (viscous resistance), and inertial resistance coefficients were assigned based on the measured bulk density of the paddy.

Table 1. Summary of boundary conditions for the CFD simulation.

Domain Zone	Boundary Type	Parameter Setting / Value
Inlet	Velocity Inlet	Velocity magnitude: 6 m s^{-1}
		Temperature: 40 °C (308.15 K)
		Turbulen viscosity ratio
		Turbulent Intensity 5%
Upper Outlet	Pressure Outlet	Gauge pressure: 0 Pa
		Turbulen viscosity ratio
		Turbulent intensity 5%
Dryer Walls	Wall (Solid)	Adiabatic, no-slip condition
Paddy Bed	Porous Medium	Viscous resistance (1/α): 1.5 × 10^7 m^{-2}
		Inertial resistance (C2): 1.3 × 10^2 m^{-1}
		Porosity: 0.45
		Density 522 kg m^{-3}
		Specific Heat (Cp): 2028 J kg^{-1} K^{-1}
		Thermal conductivity 0.1223 W m^{-1} K^{-1}

The computational domain was configured with specific boundary conditions derived directly from the experimental data. A comprehensive summary of the applied boundary conditions and parameter settings for the CFD simulation is presented in Table 1.

2.6 CFD Validation Procedure

For validation, the simulated values were compared with experimental measurements obtained at representative observation points inside the ISD (Fig. 2(c)). Airflow velocity was validated at 8 observation points, while temperature and relative humidity were validated at 12 observation points. The 12 temperature–RH points were arranged at four radial positions, each consisting of three vertical layers corresponding to the lower, middle, and upper parts of the grain bed, as illustrated in Fig. 2(c). The agreement between simulated and measured values was evaluated using the root mean square error (RMSE) and the correlation coefficient (R). Thus, the CFD component of this study specifically validated the spatial distribution of the thermo-aerodynamic parameters (airflow, temperature, and RH), without directly modeling the mass-transfer kinetics of the grain drying process itself.

3. Results and Discussion

3.1. Controlled operating conditions of the improved ISD

The measured operating performance of the improved ISD (the structural configuration and airflow pathways of which are illustrated in Figs. 1 and 2) is summarized in Table 2.

Table 2. Controlled operating conditions of the improved ISD during paddy drying.

Parameter	Mean (±SD)
Ambient temperature (°C)	32.91 ±0.68
ISD temperature (°C)	37.13 ±0.66
Ambient relative humidity (%)	66.76 ±4.08
ISD relative humidity (%)	57.32 ±8.77
Inlet air velocity (m s^{-1})	5.35 ±0.34
Air velocity at measurement points (m s^{-1})	5.28 ±0.73

Across the three drying trials, the improved ISD produced relatively consistent thermal and airflow conditions. Quantitatively, the system maintained an average internal temperature of 37.13 ± 0.66 °C, providing a stable temperature increase of approximately 4.22 °C above the ambient air (32.91 ± 0.68 °C). Furthermore, the relative humidity inside the ISD (57.32 ± 8.77%) was substantially reduced by an average of 9.44 percentage points compared to the ambient air (66.76 ± 4.08%). This measurable temperature increase and RH reduction confirmed that the system successfully provided a more favorable drying potential than the ambient environment. The dynamic profiles of these operating conditions throughout the daily drying periods are visually illustrated in Fig. 3, further confirming the stability of the thermo-aerodynamic environment inside the chamber.

Airflow measurements further showed that the controlled system maintained a relatively stable air supply during blower operation. The average inlet air velocity during blower-on periods was 5.35 ± 0.34 m s^{-1}. The low variability across trials indicated moderate-to-high stability in airflow delivery generated by the automated control system. Meanwhile, the measured air velocity at the internal observation points exhibited an average of 5.28 ± 0.73 m s^{-1}. These results suggest that the improved combination of heat exchanger, axial blower, plenum chamber, and perforated air-distribution system was capable of supplying measurable and reasonably stable airflow to the drying chamber.

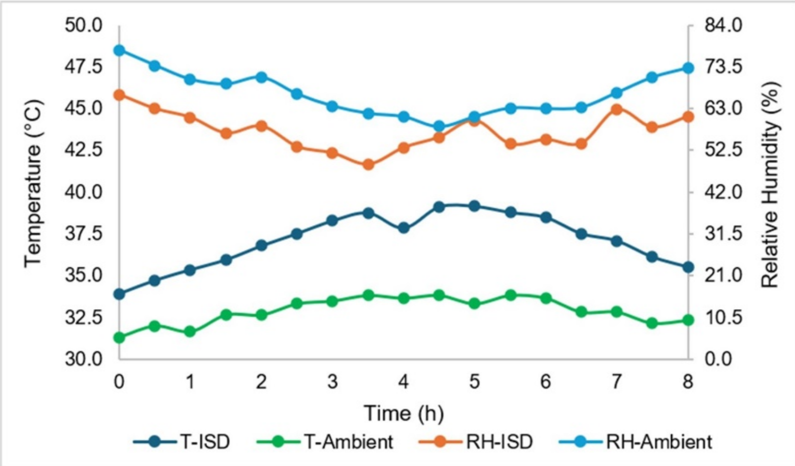

Fig. 3. Profiles of ambient and internal ISD temperature and relative humidity during the drying process.

The mean duration of blower operating modes during the 8-h drying process is presented in Table 3. Rather than running continuously at maximum capacity, the blower operated predominantly in low (47.9% of total time) and medium (37.5%) modes, while high-speed operation was triggered for only approximately 14.6% of the duration. This behavior confirms that the system actively regulated the airflow supply in response to the real-time-thermal-humidity conditions. From an engineering perspective, such dynamic behavior is highly desirable because effective drying does not strictly require maximum continuous airflow; rather, it requires sufficient airflow supplied under favorable drying conditions [18,23–25].

Table 3. Blower operation time and speed settings during paddy drying.

Blower mode	Speed (m s^{-1})	Mean duration (h) (SD)	(% of total time)
Low	5.0	3.8 ±1.0	47.9
Medium	5.5	3.0 ±0.9	37.5
High	6.0	1.2 ±0.3	14.6

Overall, the controlled operating data in Table 2. and Table 3 indicate that the improved ISD was able to maintain drying air that was warmer and generally drier than ambient air while providing stable airflow into the chamber. This is important because, in deep-bed drying systems, the quality of inlet air is one of the main determinants of moisture-removal potential [7,8,13]. Therefore, even without direct baseline data from the pre-modification configuration, the present results demonstrate that the improved system was capable of producing controlled operating conditions suitable for paddy drying.

3.2.Bulk moisture reduction and drying performance

The bulk drying performance of paddy in the improved ISD is summarized in Table 4. In the present study, the drying experiment was conducted from 09:00 to 17:00. For consistency in data presentation, the drying progress is expressed in this paper as drying time from 0 to 8 h, where 0 h corresponds to the start of drying at 09:00. Under these conditions, the improved ISD achieved substantial bulk moisture reduction during the 8-h drying period.

Table 4. Moisture reduction and drying performance of paddy in the improved in-store dryer (ISD).

Parameter	Mean (SD)
Initial moisture content (% w.b.)	17.78 ±0.39
Final moisture content (% w.b.)	10.44 ±0.38
Moisture reduction (% points)	7.33 ±0.67
Apparent moisture reduction rate (percentage points h^{-1})	0.92 ±0.24

As shown in Table 4, the initial moisture content of the paddy averaged 17.78 ± 0.39% (w.b.), while the final moisture content dropped to 10.44 ± 0.38% (w.b.). This corresponded to an average moisture reduction of 7.33 ± 0.67 percentage points, with an overall apparent moisture reduction rate of 0.92 ± 0.24 percentage points h^{-1}. On a water-removal basis, the drying process evaporated approximately 24.59 kg of water from the 300 kg paddy load, corresponding to an average mass-based drying rate of 3.07 kg H_2O h^{-1}. From a practical standpoint, the final moisture content was below the commonly recommended moisture level for storage [2,7,8], indicating that the system was able to reduce paddy moisture to a storage-safe range prior to storage [2,3]. However, further assessment of milling quality and fissuring would be required to evaluate grain-quality preservation.

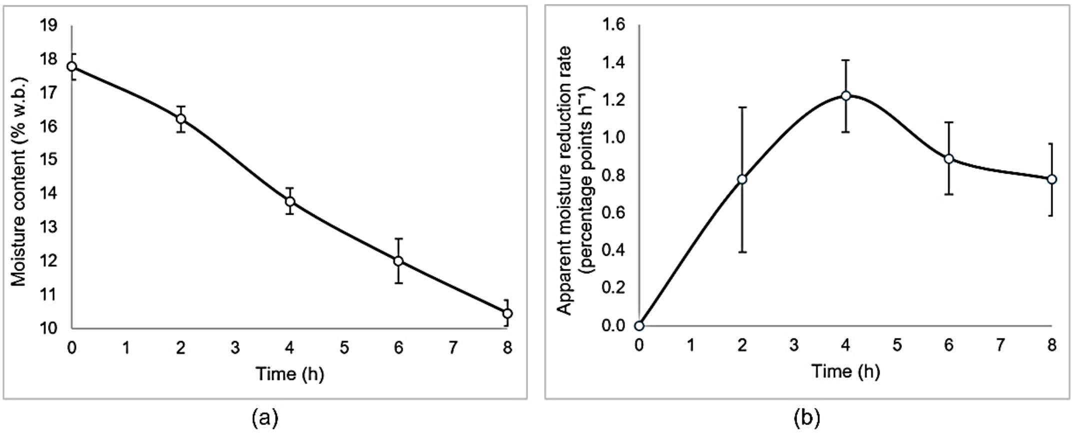

Fig. 4. Drying kinetics of paddy in the improved ISD: (a) bulk moisture content over time and (b) apparent moisture reduction rate over consecutive 2-h intervals. Data points represent mean values, and error bars indicate standard deviation.

The reduction in bulk moisture content as a function of drying time is shown in Fig. 4(a), while the corresponding numerical values are presented in Table 4. The average moisture content decreased from 17.78% at 0 h to 16.22% at 2 h, 13.78% at 4 h, 12.00% at 6 h, and 10.44% at 8 h.

This trend confirms that moisture removal proceeded continuously throughout the drying period. A more pronounced decrease occurred during the middle stage of drying, particularly between 2 and 6 h, indicating that the thermal-airflow conditions in the chamber were more favorable during that period.

The variation in the apparent moisture reduction rate during the process is visually illustrated in Fig. 4(b). As indicated by the figure, the rate did not remain constant but increased during the early stage of drying, reached its highest value in the middle of the drying period, and then gradually decreased toward the end of drying. The highest mean rate, 1.22 percentage points h^{-1}, occurred during the 2–4 h interval. The rate then decreased to 0.89 percentage points h^{-1} during 4–6 h and further to 0.78 percentage points h^{-1} during 6–8 h. This rise-and-fall pattern is consistent with the drying behavior of grain materials, in which moisture removal may intensify after the initial heating and airflow stabilization period, and then decline as grain moisture content decreases and the driving force for moisture migration becomes smaller [7,8,13,27].

Taken together, the data show that the improved ISD maintained drying conditions under which moisture reduction progressed continuously and effectively over the 8-h operation. Furthermore, the low standard deviation (±0.38%) observed in the final moisture content, derived from samples collected across the lower, middle, and upper layers of the grain bed, indicates that a reasonably uniform drying process was achieved throughout the bulk.

3.3.Energy requirement of the controlled drying process

The electrical and biomass energy consumption during controlled drying is summarized in Table 5, while the derived water-removal and energy-performance indicators are presented in Table 6. Electrical energy consumption ranged from 10.70 to 10.99 kWh per process, with an overall mean of 10.86 ± 0.15 kWh per process. Biomass consumption averaged 20 kg per process, corresponding to an averaged biomass energy input of 472.20 ± 23.61 MJ per process.

Table 5. Electrical and biomass energy consumption during controlled drying.

Parameter	Mean (SD)
Electrical energy consumption (kWh $process^{-1}$)	10.86 ±0.15
Biomass consumption (kg $process^{-1}$)	20 ±1
Biomass energy input (MJ $process^{-1}$)	472.20 ±23.6

Based on the mean reduction in bulk moisture content from 17.78% to 10.44% (w.b.) for a 300 kg paddy load, the drying process removed approximately 24.56 ± 2.14 kg of water. This corresponds to a mean mass-based drying rate of 3.07 ± 0.27 kg H_2O h^{-1}, in addition to the apparent moisture reduction rate of 0.92 percentage points h^{-1} reported earlier.

Using the average electrical energy consumption of 10.86 kWh per process, equivalent to 39.10 ± 0.53 MJ, the specific energy consumption based on electricity alone was 1.60 ± 0.12 MJ kg^{-1} water evaporated. In addition, the specific moisture extraction rate (SMER) based on electrical energy was 2.26 ± 0.17 kg H_2O kWh^{-1}. However, because thermal energy was supplied mainly by biomass, the electrical SMER should not be interpreted as the total system energy efficiency.

When the biomass energy input was included, the SEC associated with biomass energy was 19.38 ± 2.66 MJ kg^{-1} water evaporated, resulting in an estimated total SEC of 20.98 ± 2.66 MJ kg^{-1} water evaporated for the improved ISD. This total SEC is consistent with the quantitative range reported for experimental and laboratory-scale paddy drying systems (20.87 ± 14.97 MJ kg^{-1} water evaporated), although it remains higher than that of highly optimized industrial drying systems, which typically operate at significantly lower energy consumption (5.57 ± 2.21 MJ kg^{-1} water evaporated) [2]. The relatively high SEC may be associated with the use of total energy input (electricity plus biomass) [14,20], the moderate amount of water removed, and the thermal-airflow losses inherent to the present configuration [2], similar to thermal inefficiencies observed in conventional stationary beds without recirculation [5] or biomass systems lacking heat recovery components [15,19]. Additionally, empirical observations during the experiments indicated that the manual batch-feeding mechanism of the wood charcoal inherently caused transient thermal fluctuations and parasitic heat losses (e.g., cold air infiltration during furnace door opening). This manual operation prevented the system from achieving continuous steady-state combustion efficiency, which further contributed to the elevated biomass energy requirement.

Table 6. Energy performance and water removal indicators for the improved ISD.

Parameter	Mean value (SD)
Water evaporated (kg)	24.56 ±2.14
Mass-based drying rate (kg H_2O h^{-1})	3.07 ±0.27
Electrical energy consumption (kWh $process^{-1}$)	10.86 ±0.15
Electrical energy input (MJ $process^{-1}$)	39.08 ±0.53
Biomass energy input (MJ $process^{-1}$)	472.20 ±23.61
Total energy input (MJ $process^{-1}$)	511.28 ±23.09
SEC based on electricity only (MJ kg^{-1} water evaporated)	1.60 ±0.12
SEC based on biomass energy (MJ kg^{-1} water evaporated)	19.38 ±2.66
Total SEC (MJ kg^{-1} water evaporated)	20.98 ±2.78
SMER based on electricity only (kg H_2O kWh^{-1})	2.26 ±0.17

These results indicate that the improved ISD required both electrical and thermal energy inputs to maintain controlled drying operation. The electrical component mainly supported airflow generation and control, whereas the biomass component supplied the thermal energy required to increase the drying-air temperature above ambient level. From an engineering perspective, the energy indicators obtained in this study show that the improved ISD achieved substantial moisture removal under controlled operating conditions, although further improvements in heat utilization and airflow efficiency would still be desirable [2,5,29]. Overall, the results in Table 5 and Table 6 indicate that the improved ISD combined effective bulk drying performance with clearly documented energy input and drying-efficiency indicators.

3.4.CFD simulation of thermo-aerodynamic behavior

The CFD computational domain used in this study is shown in Fig. 2. The simulation represented the internal airflow region of the circular-pipe conical-floor ISD and used experimentally measured operating conditions as boundary conditions. In the present study, CFD was employed to analyze the airflow pathway and thermo-aerodynamic distribution inside the improved dryer [4,9,11,26].

The CFD contour plots indicate that heated air entered the plenum chamber from the heat-exchanger section and was distributed upward through the perforated inlet air pipes and the perforated conical floor into the grain bulk [4,9,11]. Because the inlet air pipes were arranged radially and the conical floor formed the lower airflow-supporting structure, the system promoted multidirectional airflow distribution within the drying chamber rather than a simple one-directional vertical flow [9–11]. Specifically, based on the vector plots, this dominant multidirectional pattern consisted of upward flow from the plenum, radial spreading from the perforated pipes, and local circulation toward the suspended outlet pipes.

The velocity contours (Fig. 5(b)) show that the predicted airflow velocity ranged from 0.00 to 7.35 m s^{-1} within the chamber, with the highest values near the inlet-pipe outlets and lower values in the upper peripheral zones. This pattern indicates that the inlet-pipe system functioned effectively as the main pathway for delivering drying air into the grain bed.

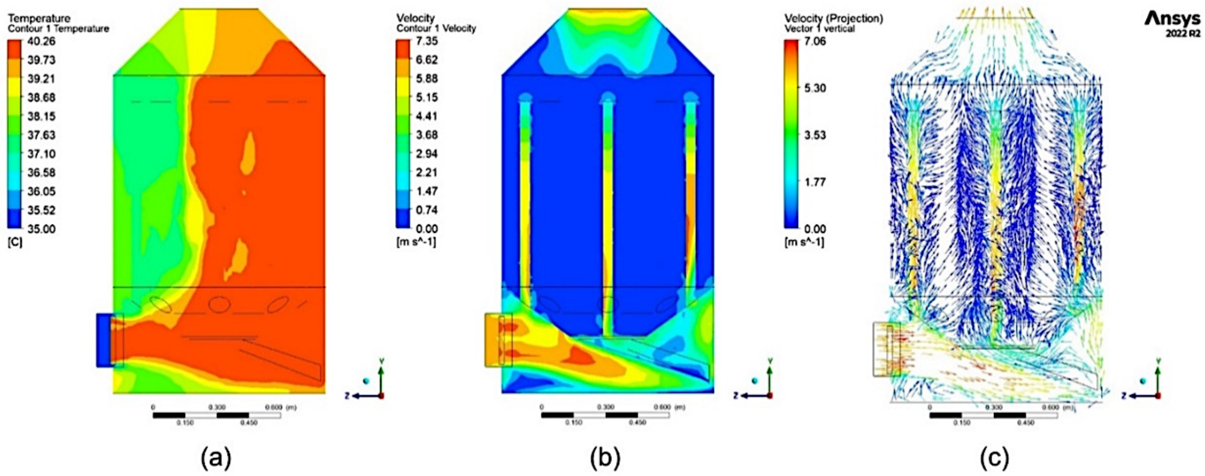

Fig. 5. CFD-predicted thermo-aerodynamic distribution in the improved ISD: (a) temperature contour, (b) airflow velocity contour, and (c) airflow vector field (side views).

The temperature contours (Fig. 5(a)) further show that thermal energy was distributed throughout the chamber, although local non-uniformity remained in several regions. The lower part of the chamber, particularly near the plenum and air-distribution system, tended to have higher temperatures, while some upper regions showed relatively lower values. This pattern suggests that the circular-pipe conical-floor configuration was able to distribute heated air through most of the grain bed while still producing local gradients associated with airflow pathway and outlet direction. In addition, the airflow contours and vector plots (Fig. 5(b-c)) support the role of the circular-pipe and conical-floor structure in promoting radial and vertical air distribution inside the ISD.

3.5. Validation of the CFD model

Model validity was assessed by comparing CFD-predicted temperature, relative humidity, and airflow velocity with experimental measurements at representative observation points in the grain bulk. Temperature and relative humidity were validated at 12 points distributed over four radial positions and three vertical layers (lower, middle, and upper), while airflow velocity was validated at 8 points. The corresponding comparisons are shown in Fig. 6(a), Fig. 6(b), and Fig. 6(c), respectively.

The agreement between simulated and measured values was evaluated using the root mean square error (RMSE) and the correlation coefficient (R), and the validation statistics are summarized in Table 7. For temperature validation, the CFD model showed good agreement with the measured data, with an RMSE of 0.54 °C and a correlation coefficient of 0.81. The mean bias was −0.12 °C, indicating that the model slightly underpredicted the measured temperature while still reproducing the internal thermal condition of the ISD with satisfactory accuracy.

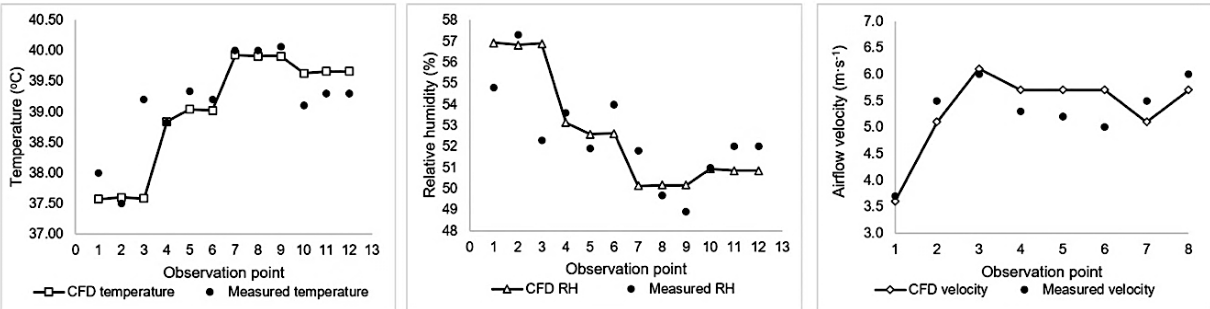

Fig. 6. Validation of CFD-predicted and measured (a) temperature, (b) RH and (c) airflow velocity at representative observation points in the grain bed of the ISD.

As shown in Fig. 6(a), the predicted and measured temperature values followed a similar pattern across the observation points. However, residual analysis revealed a localized deviation, particularly at observation point 3, where the CFD model underpredicted the temperature. Physically, this point was located in the upper layer at the front section closest to the blower, situated directly between the perforated inlet and suspended outlet pipes. This zone is highly susceptible to localized hot-air channeling or "short-circuiting", where the actual hot and dry air swiftly bypasses the grain bulk, resulting in a hotter physical condition than predicted. Conversely, observation point 10 (located at the bottom layer, between the central inlet pipe and two outlet pipes on the right side) exhibited a slight temperature overprediction. In reality, this bottom zone likely experienced localized airflow stagnation or higher grain compaction, causing lower actual heat transfer. The uniform porous medium assumption in the standard CFD model inherently smoothed out these micro-scale channeling and stagnation effects, leading to the localized residuals observed [4,9,11].

Table 7. Validation statistics for CFD-predicted temperature, relative humidity, and airflow velocity against experimental measurements.

Variable	Mean CFD	Mean measured	Bias	RMSE	R
Temperature (°C)	39.03	39.15	-0.12	0.54	0.81
Relative humidity (%)	52.68	52.45	0.23	1.73	0.76
Airflow velocity (m s^{-1})	5.34	5.28	0.06	0.38	0.84

For relative humidity validation, the CFD model also showed acceptable agreement with the measured values, with the validation statistics summarized in Table 7. The model yielded an RMSE of 1.73%, a correlation coefficient of 0.76, and a mean bias of 0.23%. As shown in Fig. 5(b), the predicted and measured RH values followed a generally similar pattern across the observation points. Although local deviations remained at several points (such as a corresponding RH overprediction at observation point 3 due to the localized hot-air channeling mentioned previously), the predicted RH distribution was overall consistent with the measured drying conditions inside the ISD.

For airflow velocity, the CFD model yielded the highest agreement among the validated variables, as summarized in Table 7, with an RMSE of 0.38 m s^{-1}, a correlation coefficient of 0.84, and a mean bias of 0.06 m s^{-1}. As shown in Fig. 6(c), the predicted airflow velocity followed the measured values closely across the observation points, including the lower velocity at one point and the higher values at the others. This result indicates that the CFD model was able to reproduce the airflow pathway in the improved ISD with good accuracy.

Overall, the validation results presented in Fig. 6 indicate that the CFD model was able to reproduce the internal distribution of temperature, relative humidity, and airflow velocity in the improved ISD. As indicated by the correlation coefficients, the RH prediction (R = 0.76) and temperature prediction (R = 0.81) represent moderate to good agreement, whereas the velocity prediction (R = 0.84) shows stronger agreement. This provides two important implications. First, it allows the internal airflow pathway of the improved ISD to be interpreted with greater confidence. Second, it demonstrates that the numerical model was capable of representing the internal drying conditions of the ISD. Accordingly, the CFD component of this study should be regarded not merely as a qualitative visualization tool but as a validated chamber-scale model for the improved circular-pipe conical-floor ISD under the specific operating condition tested in this study [9,11]. The authors avoid overclaiming the model as broadly validated across all possible drying scenarios but emphasize its reliability for the parameters investigated herein.

From an engineering standpoint, the validated CFD model supports the experimental findings presented in Table 7 and Fig. 6, showing that the improved ISD was capable of maintaining airflow and thermal-humidity conditions that enabled effective bulk moisture reduction during the 8-h drying period. The agreement between simulated and measured data across the lower, middle, and upper layers indicates that the model can adequately describe the internal behavior of the dryer under the tested operating condition. Although broader validation under additional operating scenarios would further strengthen the general applicability of the model, the present CFD results already provide a strong basis for explaining the airflow, temperature, and RH distribution in the improved ISD.

3.6.Practical implication of the improved ISD design

The improved ISD configuration shown in Fig. 1 and Fig. 2 offers several practical engineering advantages. First, the use of a perforated conical floor and perforated inlet-air pipes provides a structured pathway for air supply from the plenum chamber into the grain bulk [9–11]. This arrangement facilitates radial distribution of drying air rather than limiting the system to a single localized inlet region [9,10]. Second, the suspended outlet pipes are expected to facilitate the removal of moist air from the grain bulk, although further quantitative analysis of residence time or humidity accumulation would be needed to confirm their effect on stagnation.

Third, the integration of a biomass furnace, heat exchanger, and axial blower makes the system suitable for controlled drying under conditions where ambient air alone may not be sufficient [2,14,15]. This is particularly relevant in environments where ambient RH fluctuates and additional heating is needed to improve drying potential [2,3,20]. The operating data presented in Tables 2 and 5 indicate that the system was able to produce an internal drying condition that was warmer and generally drier than ambient air while still maintaining repeatable airflow characteristics.

From the standpoint of grain handling, the final moisture content achieved Table 4 indicates that the ISD can function effectively as a paddy drying unit prior to storage. Because the dryer also includes a paddy discharge outlet and an integrated storage-oriented chamber design, it offers operational flexibility for postharvest handling. Such characteristics make the system relevant not only as an experimental dryer but also as a practical technology platform for controlled grain drying in agricultural applications.

3.7. Limitation of the present analysis

The limitations of the present study should be understood in relation to the development stage of the ISD system. The earlier ISD study before axial-blower modification mainly provided a reference for hot-air supply performance, including chamber temperature, RH behavior, and inlet–outlet airflow velocity, and also identified the need to regulate blowing speed to reduce temperature fluctuation and improve heat delivery [6].

To be fully explicit regarding the scope, this study acknowledges three primary limitations. First, the present study did not conduct a strict before-and-after comparison of drying performance indicators with the previous dryer configuration but rather focused on evaluating the improved configuration developed after that stage. Second, while the CFD model was validated using representative measurements of temperature, relative humidity, and airflow velocity, this validation was limited to the specific operating condition tested in this study. Third, post-drying grain-quality indicators, such as fissuring, head rice yield, and milling quality, were not evaluated.

Broader operating scenarios, denser spatial validation, and more explicit evaluation of heat-loss reduction in the heat-exchanger section, alongside comprehensive grain-quality assessments, would further strengthen the general applicability of the model and the engineering interpretation of the improved ISD. Furthermore, upgrading the current manual charcoal-feeding method to an automated continuous-feeding system is highly recommended for future designs to minimize combustion fluctuations and improve overall thermal efficiency.

4. Conclusions

The circular-pipe conical-floor in-store dryer (ISD) demonstrated its feasibility as a paddy drying system equipped with an improved hot-air supply arrangement and validated CFD-based airflow analysis. Under the tested operating condition, the system maintained relatively stable thermal and airflow characteristics and reduced paddy moisture content from 17.78% to 10.44% (w.b.) within 8 h, corresponding to an apparent moisture reduction rate of 0.92 percentage points h^{-1}. On a water-removal basis, the process removed approximately 24.59 kg of water from a 300 kg paddy load, equivalent to a mass-based drying rate of 3.07 kg H_2O h^{-1}.

The average energy input per process consisted of 39.08 MJ of electrical energy (equivalent to 10.86 kWh) and 472.20 MJ of biomass thermal energy. This combined energy input resulted in an estimated total specific energy consumption of 20.98 MJ kg^{-1} water evaporated. These results indicate that the improved ISD achieved substantial bulk moisture reduction under a measurable and repeatable energy requirement. The CFD model successfully reproduced the internal distribution of temperature, relative humidity, and airflow velocity with acceptable to good agreement with the experimental data. The validation results showed RMSE values of 0.54 °C for temperature, 1.73% for relative humidity, and 0.38 m s^{-1} for airflow velocity, with corresponding correlation coefficients of 0.81, 0.76, and 0.84, respectively. This confirms that the CFD model can adequately represent the internal drying conditions of the improved ISD under the tested operating regime.

Overall, the study shows that the performance of the improved ISD depends not only on the chamber geometry but also on the effectiveness of hot-air delivery into the plenum and grain bed.

Further work should include broader operating scenarios, denser spatial validation, and a more detailed thermal-loss analysis, and post-drying grain-quality assessments to improve the general applicability and energy efficiency of the system.

Abbreviations

-

Data Availability Statement

Data will be shared upon request by the readers.

CRediT Authorship Contribution Statement

Diswandi Nurba: Conceptualization, Methodology, Investigation, Data curation, Formal analysis, Software, Visualization, Writing – original draft. **Muhammad Yasar**: Supervision, Validation, Methodology, Writing – review and editing. **Dyah Wulandani:** Conceptualization, Methodology, Validation, Supervision, Formal analysis, Writing – review and editing.

Declaration of Competing Interest

The authors of this manuscript declare no conflict of interest or competing interest.

Declaration of Use of AI in the Writing Process

Nothing to disclose.

Acknowledgement

This work was supported by the Lecturer Research Scheme of Universitas Syiah Kuala under Contract No. 167/UN11.2.1/PT.01.03/PNBP/2021. The experimental in-store dryer (ISD), including its heat exchanger and input-air control system, was developed and utilized under this research project.

References

[1] Wang J, Wang D, Zhan T, Qiu S, Tao D, Ji D, et al. Effect of tempering drying on the physicochemical properties of paddy rice. J Food Process Preserv 2022;46:e16374. https://doi.org/10.1111/JFPP.16374.

[2] Ying T, Spang ES. Paddy Drying Technologies: A Review of Existing Literature on Energy Consumption. Processes 2024;12:532. https://doi.org/10.3390/PR12030532.

[3] Duangkhamchan W, Huangsaeng K, Kondo N, Jaisut D. Enhancing Paddy Rice Preservation in Small-Scale Barns: Comparative Analysis of Hot Air-Drying Techniques and Ventilation Impact on Quality and Energy Efficiency. Foods 2024;13:672. https://doi.org/10.3390/FOODS13050672.

[4] Li B, Feng S, He Q, Zhu Y, Hu Z, Jiang Y, et al. Numerical simulation of rice drying process in a deep bed under an angular air duct. J Food Process Eng 2023;46:e14438. https://doi.org/10.1111/JFPE.14438.

[5] Wang G, Wu W, Fu D, Xu W, Xu Y, Zhang Y. Energy and Exergy Analyses of Rice Drying in a Novel Electric Stationary Bed Grain-Drying System with Internal Circulation of the Drying Medium. Foods 2022;11:101. https://doi.org/10.3390/FOODS11010101.

[6] Nurba D, Yasar M, Mustaqimah, Fadhil R, Sari SP, Mysa CV. Performance of corncobs and wood charcoal briquette as heat energy sources in In-Store Dryer. IOP Conf. Ser. Earth Environ. Sci 2019;365. https://doi.org/10.1088/1755-1315/365/1/012048.

[7] Brooker DB, Bakker-Arkema FW, Hall CW. Drying and storage of grains and oilseeds. New York: Springer New York 1992. https://books.google.co.id/books?id=qx-BaufhXKoC&printsec=copyright&hl=id#v=onepage&q&f=false
[8] Mujumdar AS. Handbook of Industrial Drying. Boca Raton (US): CRC Press 2014. https://doi.org/10.1201/b17208
[9] Nurba D, Mardjan SS, Wulandani D, Nelwan LO, Subrata IDM. Evaluation of airflow, temperature, and RH in the deep bed dryer for paddy grain with several combinations of floors and air distribution pipes using CFD. IOP Conf Ser Earth Environ Sci 2024;1386:012002. https://doi.org/10.1088/1755-1315/1386/1/012002.
[10] Nurba D, Mardjan SS, Wulandani D, Nelwan LO, Subrata IDM. Aeration system optimization for a deep bed dryer for paddy grain using computational fluid analysis and the AHP-TOPSIS method. Engineering Agriculture 2025;12:308. https://doi.org/10.15302/J-FASE-2024577.
[11] Revilla AB, Honra J. CFD simulation of drying rice paddy in a deep-bed dryer with inclined false floor 2024;13285:60–7. https://doi.org/10.1117/12.3050567.
[12] Cnossen AG, Siebenmorgen TJ. The glass transition temperature concept in rice drying and tempering: effect on milling quality. Transactions of the ASAE 2000;43:1661–7. https://doi.org/10.13031/2013.3066.
[13] Jimoh KA, Hashim N, Shamsudin R, Man HC, Jahari M, Onwude DI. Recent Advances in the Drying Process of Grains. Food Engineering Reviews 2023;15:548–76. https://doi.org/10.1007/S12393-023-09333-7.
[14] Yahya M, Fahmi H, Hasibuan R. Experimental Performance Analysis of a Pilot-Scale Biomass-Assisted Recirculating Mixed-Flow Dryer for Drying Paddy. Int J Food Sci 2022;2022:4373292. https://doi.org/10.1155/2022/4373292.
[15] Yahya M, Fahmi H, Hadi S, Edison. Performance analyses on fluidized bed dryer integrated biomass furnace with and without air preheater for paddy drying. International Journal of Power Electronics and Drive Systems (IJPEDS) 2019;10:1555–63. https://doi.org/10.11591/IJPEDS.V10.I3.PP1555-1563.
[16] Lamidi RO, Jiang L, Pathare PB, Wang YD, Roskilly AP. Recent advances in sustainable drying of agricultural produce: A review. Appl Energy 2019;233:367–85. https://doi.org/10.1016/j.apenergy.2018.10.044.
[17] Mohapatra SS, Mahanta P. Performance Evaluation of Quality Drying in a Natural Convection Grain Dryer. Applied Mechanics and Materials 2012;110–16. https://doi.org/10.4028/www.scientific.net/AMM.110-116.2094.
[18] Sun J, Xu Y, Zhu X, Zhang W, Cao X. Intelligent Control Framework for Biomass Drying Process with Flue Gases Based on FLC and CAN Bus. Proceedings of the 4th IIAE International Conference on Industrial Application Engineering 2016 https://doi.org/10.12792/iciae2016.036.
[19] Yahya M. Performance Analysis of Solar Assisted Fluidized Bed Dryer Integrated Biomass Furnace with and without Heat Pump for Drying of Paddy. International Journal of Photoenergy 2016;2016:3801918. https://doi.org/10.1155/2016/3801918.
[20] Mihret YC, Delele MA, Hailemesikel ST. Design, development, and testing of rice-husk fueled mixed-flow rice dryer for small-scale rice producer farmers. Heliyon 2023;9:e18077. https://doi.org/10.1016/J.HELIYON.2023.E18077.
[21] Duarte LEV, Gamboa FM, López JRE. Proposal for improving of paddy rice drying process in dryers inclined pools. Scientia et Technica 2021;26:146–51. https://doi.org/10.22517/23447214.24554.
[22] Delgado-Plaza E, Quilambaqui M, Peralta-Jaramillo J, Apolo H, Velázquez-Martí B. Estimation of the Energy Consumption of the Rice and Corn Drying Process in the Equatorial Zone. Applied Sciences 2020;10:7497. https://doi.org/10.3390/app10217497.

[23] Zhang L, Cui H, Li H, Han F, Zhang Y, Wu W. Parameters Online Detection and Model Predictive Control during the Grain Drying Process. Math Probl Eng 2013;2013:924698. https://doi.org/10.1155/2013/924698.

[24] Dai A, Zhou X, Wu Z. Design of an intelligent controller for a grain dryer: A support vector machines for regression inverse model proportional–integral–derivative controller. Food Sci Nutr 2020;8:805–19. https://doi.org/10.1002/FSN3.1340.

[25] Zhang Y, Fang Z, Li C, Li C. Deep-Learning-Based Model Predictive Control of an Industrial-Scale Multistate Counter-Flow Paddy Drying Process. Foods 2023;13:43. https://doi.org/10.3390/FOODS13010043.

[26] Salvatierra-Rojas A, Ramaj I, Romuli S, Müller J. CFD-Simulink Modeling of the Inflatable Solar Dryer for Drying Paddy Rice. Applied Sciences 2021;11:3118. https://doi.org/10.3390/app11073118.

[27] Golpour I, Guiné RPF, Poncet S, Golpour H, Chayjan RA, Parian JA. Evaluating the heat and mass transfer effective coefficients during the convective drying process of paddy (Oryza sativa L.). J Food Process Eng 2021;44:e13771. https://doi.org/10.1111/JFPE.13771.

[28] Akhtaruzzaman M, Mondal MHT, Sarker MSH, Biswas M, Shanta SA, Sheikh MAM. Evaluation of drying characteristics, energy consumption and quality of parboiled paddy: Two stage drying. J Agric Food Res 2022;8:100284. https://doi.org/10.1016/J.JAFR.2022.100284.

[29] An J, Xie H, Yan J, Wei H, Wu Y, Liao X. A review of applications of energy analysis: Grain, fruit and vegetable drying technology. Energy Reports 2024;12:5482–506. https://doi.org/10.1016/J.EGYR.2024.11.037.